BIOCHEMISTRY
including biophysical chemistry & molecular biology
Article

Biochemistry **2009,** *48,* 8551–8558 8551
DOI: 10.1021/bi901070t

The Unfolding of the Prion Protein Sheds Light on the Mechanisms of Prion Susceptibility and Species Barrier†

Philip J. Robinson and Teresa J. T. Pinheiro*

Department of Biological Sciences, University of Warwick, Gibbet Hill Road, Coventry CV4 7AL, U.K.

Received June 24, 2009; Revised Manuscript Received August 5, 2009

ABSTRACT: Prion diseases are a group of fatal neurodegenerative disorders that manifest as infectious, sporadic, or familial and are all associated with the misfolding of the prion protein (PrP). Disease-modulating polymorphisms in the PrP amino acid sequence can make an individual more or less susceptible to infection. One example is the presence of arginine in place of glutamine at position 171 in sheep, which confers resistance to scrapie. To investigate whether the physical folding properties of PrP are influenced by the presence of arginine at codon 171, we have introduced the mutation at the equivalent position (codon 167) in recombinant mouse PrP. We have then compared the unfolding properties of wild-type PrP and the Q167R mutant by monitoring the fluorescence and circular dichroism of folding-sensitive tryptophan mutants. For both wild-type PrP and the Q167R mutant the formation of secondary structure and tertiary structure is concurrent, which indicates that unfolding proceeds without the accumulation of an equilibrium intermediate. The major effect of the mutation is the destabilization of the protein as shown by the shift of the unfolding transition, which can be rationalized from high-resolution structures of PrP. Comparison of the unfolding pathways of mouse and hamster PrP highlights dramatic differences in the mechanisms of folding, which may contribute to the species barrier effect that is observed in the transmission of prion disease.

Prion diseases are a group of fatal, protein misfolding, neurodegenerative disorders that manifest as infectious, sporadic, or familial (*1*). All of the familial diseases can be attributed to alterations of the prion gene, PRNP, that result in either amino acid substitutions, premature stop codons, or insertion of additional octarepeats in the prion protein (PrP)[1] (*2*). Disease-modulating polymorphisms in PRNP that do not result in sporadic disease can make an individual more or less susceptible to infection. In classical sheep scrapie, three codons are particularly important in influencing susceptibility; these codons are 136, 154, and 171, and the polymorphisms at these positions are A136V/T, R154H/L, and Q171R/H/K (*3*). Different combinations of these polymorphisms lead to different levels of scrapie susceptibility.

The presence of arginine at codon 171 has a dominant resistant effect on classic scrapie susceptibility; therefore, sheep that are QQ, HQ, or HH at codon 171 are susceptible to scrapie (*4*, *5*) whereas QR, HR, or RR are much more resistant (*6*). Scrapie has never been reported as a spontaneous genetic disease and therefore requires the presence of the infectious agent (*7*). The strain of the infectious agent is also important in assessing susceptibility, as different genetic backgrounds are susceptible to different strains of prion disease (*8*). However, the resistance induced by the 171R polymorphism is to our knowledge strain independent, which suggests it manifests through a more generic mechanism than the effects of the other codons.

The expression of mutant PrP in scrapie-infected neuroblastoma cells (*9*) and transgenic mice (*10*), containing the corresponding mutation (Q167R), confers resistance to prion propagation. The location of this mutation on the structure of PrP is shown in Figure 1. This mutation has been described as having a dominant inhibitory effect on prion conversion, as the product of the mutant allele interferes with conversion of the wild-type protein.

The mechanism by which R171 confers resistance to prion disease is currently unknown. In $PrP^{ARR/ARQ}$ heterozygous sheep both alleles are equally expressed, and therefore the dominance of the resistant phenotype is not due to the absence of PrP^{ARQ} (*11*). This suggests that the properties of PrP^{ARR} interfere with the conversion of the normally susceptible PrP^{ARQ}. The *in vitro* fibrillization of a different PrP dominant negative mutant, Q218K, showed that the mutation increased the lag time of fibrillization and reduced the overall yield of fibers (*12*). This indicates that the dominant negative phenotype results from the fact that the Q218K mutant is less prone to misfolding and aggregation. Another possibility is that dominant negative mutations interfere with the binding of an essential cellular cofactor for prion propagation (*9*).

Another phenomenon associated with the transmission of prion diseases is the species barrier, which results in a longer incubation time and lower incidence of disease on transfer of infection between species (*13*). It has been established that the species barrier is under control of the primary sequence of PrP (*14*), even though the mechanism of control is not understood. As the structure of PrP is highly conserved, it is unlikely that structural differences between PrP from different species are responsible. However, the fact that the primary sequence and structures are highly conserved does not necessarily mean that the folding mechanism is also conserved. Therefore, comparing the

†This project was funded by the Biotechnology and Biological Sciences Research Council, grant BB/D524516/1, and studentship 88/DTA19176.

*Address correspondence to this author. Tel: +44 (0) 2476 528364. Fax: +44 (0) 2476 523701. E-mail: t.pinheiro@warwick.ac.uk.

[1]Abbreviations: PrP, prion protein; MoPrP, mouse prion protein; CD, circular dichroism; NMR, nuclear magnetic resonance.

Published on Web 08/05/2009

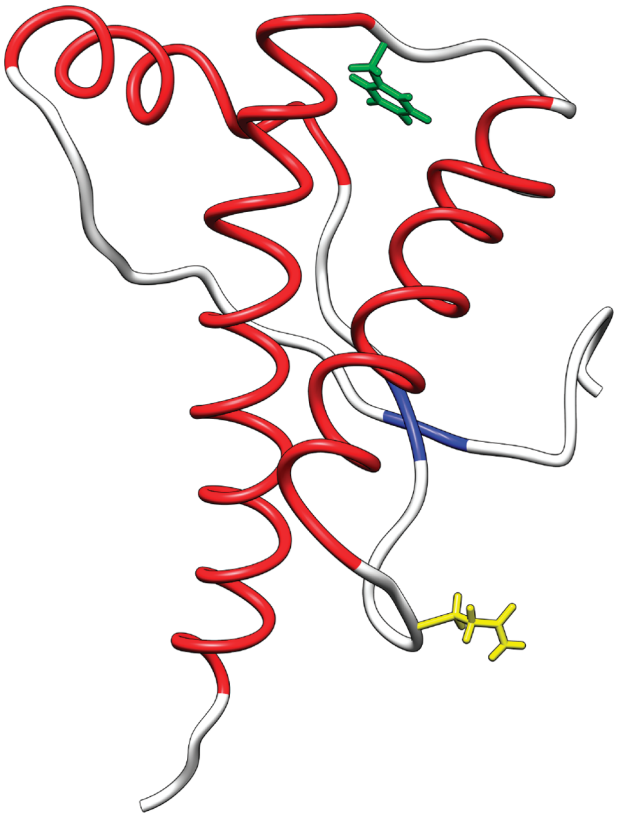

FIGURE 1: The structure of the globular domain of the mouse prion protein. Ribbon representation of the MoPrP structure (residues 120−230), highlighting the positions of Q167 (yellow) and F197 (green). Helices are shown in red, and a small antiparallel β-sheet is in blue. The NMR structure (*36*) was drawn from the PDB file 1XYX using the UCSF Chimera package from the Resource for Biocomputing, Visualization and Informatics at the University of California, San Francisco (supported by NIH P41 RR-01081) (*48*).

folding properties of PrP from different species may give insight into the mechanism of the species barrier.

The misfolding of globular proteins is considered to be initiated by partial or global protein unfolding (*15*). Therefore, studying the folding properties of PrP may help us to understand the misfolding mechanisms associated with disease. To investigate whether the physical folding properties of PrP are influenced by the Q167R mutation, we will compare the unfolding of wild-type PrP to the Q167R mutant. The aim is to see if the mutation alters the unfolding mechanism of PrP, which includes the overall stability of the protein fold and the effects on intermediate species on the folding pathway.

Thermal unfolding of wild-type PrP and the Q167R mutant will be followed through circular dichroism (CD). Then a folding-sensitive tryptophan mutant (F197W) will be used to follow the urea-induced unfolding of PrP, and this will be compared to F197W/Q167R, the same folding-sensitive mutant with the Q167R mutation. These data will also be compared to equilibrium unfolding data previously collected with the hamster prion protein (*16*) to see if there is species variation in the folding properties of the prion protein, which may provide information on the mechanisms by which the primary sequence of PrP controls the species barrier.

EXPERIMENTAL PROCEDURES

Expression, Purification, and Refolding of PrP. The plasmid encoding mouse PrP(Met91−230) was provided by Prof. David Brown, University of Bath. From this plasmid folding-sensitive site-directed mutants were produced using a QuikChange kit (Stratagene, Amsterdam Zuidoost, The Netherlands) according to the manufacturer's instructions. This involved mutating the two native tryptophans (W98 and W144) to phenylalanine residues and introducing a folding-sensitive tryptophan residue at position 197 to produce PrP^{F197W}. The Q167R mutation was then introduced on the background of PrP^{Wt} and PrP^{F197W} to produce PrP^{Q167R} and $PrP^{F197W/Q167R}$.

Recombinant mouse prion protein, MoPrP(Met91−230), and all associated mutants were expressed in *Escherichia coli* BL21 Star Rosetta (Invitrogen, Paisley, U.K.) as insoluble inclusion bodies, which were isolated and solubilized as described previously for hamster PrP (*16*). The solubilized inclusion bodies were loaded onto a 26/60 Sephacryl S-300 high-resolution gel filtration column (Amersham Biosciences, Buckinghamshire, U.K.) equilibrated with 6 M guanidine hydrochloride and 100 mM Tris-HCl, pH 8. Fractions containing PrP were pooled and oxidized with copper. PrP with an oxidized disulfide bond was then separated through reverse-phase HPLC. Purified PrP was dialyzed against 5 mM MES, pH 5, to refold to a α-helical conformation as confirmed through CD before storage in aliquots at −20 °C. Protein samples were thawed prior to use, and PrP concentration was determined spectrophotometrically using a molar extinction coefficient ε_{280} of 25700 M^{-1} cm^{-1} for PrP^{Wt} and PrP^{Q167R} and 20100 M^{-1} cm^{-1} for PrP^{F197W} and $PrP^{F197W/Q167R}$ (*17*). The molecular weight of all constructs was confirmed through mass spectrometry.

Thermal Unfolding Transition Curves by Circular Dichroism. Thermal unfolding transition curves were measured on a Jasco J-815 spectropolarimeter with a Jasco PFD-425S Peltier type FDCD attachment for temperature control. For each experiment a sample of 12 μM PrP was prepared in 20 mM MOPS, pH 7, and transferred to a 1 mm path length quartz cuvette. The CD signal was recorded at 222 nm between 5 and 95 °C at a rate of 1 °C per minute and with a bandwidth of 1 nm. Data points were collected every 0.2 °C. On reaching 95 °C the process was reversed back to 5 °C to obtain the refolding transition curves.

Assuming that the unfolding process is two state and reversible, at equilibrium the free energy of folding (ΔG_F) can be represented in terms of the folding constant (K_F): $\Delta G_F = -RT \ln K_F$, where R is the gas constant (8.314 J K^{-1} mol^{-1}) and T is the absolute temperature measured in kelvin (K). The Gibbs−Helmholtz equation describes the unfolding of a monomer as a function of temperature: $\Delta G_F = \Delta H_F(1 - T/T_M) - \Delta C_p((T_M - T) + T \ln(T/T_M))$, where ΔG_F is the free energy of folding, ΔH_F is the enthalpy of folding, T is the temperature, T_M is the temperature at which half the protein is unfolded, and ΔC_p is the change in heat capacity when going from the folded to the unfolded state (*18*). Taking the value of ΔC_p as zero, this relationship was used to fit the change in mean residue ellipticity at 222 nm as a function of temperature through nonlinear least-squares analysis using SigmaPlot (Systat Software, Richmond, CA). Corrections were applied to take into account the sloping pretransition baseline that is clearly observed for the unfolding of PrP.

Thermal Unfolding Far-UV CD Spectra. Complete far-UV CD spectra (185−260 nm) were measured at temperatures selected along the thermal unfolding transition curves measured at 222 nm. For each series of spectra, a sample of 12 μM PrP was prepared, in 5 mM MOPS, pH 7, and transferred to a 1 mm path length quartz cuvette. A spectrum was initially measured at 5 °C,

and then the temperature was increased stepwise up to 90 °C. Typically, a scanning rate of 100 nm/min, a time constant of 1 s, and a bandwidth of 1.0 nm were used, with a resolution of 0.5 nm and 16 scans averaged per spectrum. The corresponding buffer backgrounds were subtracted from the final spectra.

Fluorescence Denaturant Unfolding. For each fluorescence experiment a folded and unfolded stock of 5 μM PrP was prepared. The folded stock was prepared in 20 mM MOPS, pH 7, and the unfolded stock was prepared in 8.5 M urea and 20 mM MOPS, pH 7. A stock solution of 10 M urea was made up fresh and treated with Amberlite deionizing resin (Merck, Darmstadt, Germany) for 12−16 h. In a typical unfolding experiment an aliquot of the folded stock was removed from a 1 cm path length quartz cuvette and replaced with an aliquot of the same volume of the unfolded stock, so that the protein concentration remained the same but the concentration of urea increased for each measurement. Fluorescence spectra were recorded at 20 °C on a Photon Technology International spectrofluorometer. The samples were excited at 295 nm (4 nm bandwidth), and emission spectra were collected between 305 and 450 nm (2 nm bandwidth). Two scans were averaged per spectrum, and corresponding buffer blanks were collected and subtracted.

Unfolding curves were obtained by following the change in the λ_{max} of the fluorescence spectrum with increasing urea concentrations. In order to calculate the free energy of folding in the absence of denaturant (ΔG_0), the linear extrapolation method was used (*19*). This assumes that the experimentally observed values for the free energy of folding (ΔG_i) over the transition region of the folding curve are linearly dependent on denaturant concentration: $\Delta G_i = \Delta G_0 - m$[denaturant], where m is a constant, which reflects the gradient of a plot of ΔG_i against denaturant concentration. This relationship can then be extrapolated to zero denaturant concentration in order to define ΔG_0. By this method the folding constant K_F at specific concentrations of denaturant can be written as $K_F = e^{-(\Delta G_0 - m[\text{denaturant}]/RT)}$. The data were fit to two-state transition curves by nonlinear least-squares regression using Sigmaplot (Systat Software, Richmond, CA), taking into account the slopes observed in the preunfolding baseline.

Normalizing Unfolding Transition Curves. Estimates of the molar ellipticity (CD experiments) or the shift in λ_{max} (fluorescence experiments) for the fully folded (y_F) and fully unfolded (y_U) protein were calculated from the fits of the raw data and used to normalize each data set to the fraction of protein unfolded (f_N): $f_N = (y - y_F)/(y_U - y_F)$, where y is the experimental parameter measured. The fraction of unfolded protein was then plotted against temperature or urea to give the unfolding transition curves that are presented.

Urea-Induced Denaturant Unfolding Monitored by Circular Dichroism. For each measurement separate samples were prepared by diluting a concentrated stock of folded PrP to 6.5 μM in 20 mM MOPS, pH 7, with varying concentrations of urea. Far-UV CD spectra were measured as stated previously but with a resolution of 1 nm, and 16 scans were averaged per spectrum. The corresponding backgrounds were subtracted from the final spectra. The ellipticity at 222 nm was determined from each far-UV CD spectrum and normalized to the fraction unfolded, taking the value at 8.5 M urea as fully unfolded and the value at 0 M urea as fully folded.

Phase Diagram Analysis of Fluorescence Unfolding. Phase diagram analysis of spectroscopic folding data can highlight the accumulation of intermediate states (*20*). The basis of the analysis is that two independent wavelengths will have a linear dependence on each other if the changes of the protein are all or none between two conformational states. If the plots are nonlinear, it indicates the presence of intermediate states. Phase diagrams were drawn by plotting the fluorescence at 320 nm against the fluorescence at 365 nm for a range of urea concentrations across the transition curve. Straight lines were fit to the plots by linear regression.

RESULTS

Protein unfolding can be monitored by any measurable property that significantly changes between the native and unfolded states (*19*). In this study PrP unfolding is followed by changes in far-UV circular dichroism and tryptophan fluorescence. The unfolding properties of wild-type PrP are compared to the Q167R mutant.

Structure of PrP Constructs. In order to create a folding-sensitive tryptophan mutant, the two native tryptophan residues at positions 98 and 144 were mutated to phenylalanine residues, and the phenylalanine residue at position 197 was mutated to tryptophan. To ensure that these mutations do not significantly alter the structure of PrP, the far-UV CD spectra of the mutants were compared to the wild-type protein. Figure 2 shows that the CD spectra of all the PrP constructs have negative bands at 208 and 222 nm and a positive band at 195 nm; these bands are characteristic of proteins that are rich in α-helix structure. The CD spectra are highly similar, which indicates that the mutations do not significantly alter the secondary structure of PrP.

Thermal Unfolding of PrP^{Wt} and PrP^{Q167R}. Thermal unfolding of wild-type PrP and the Q167R mutant was followed by far-UV CD. The 222 nm band was monitored to produce

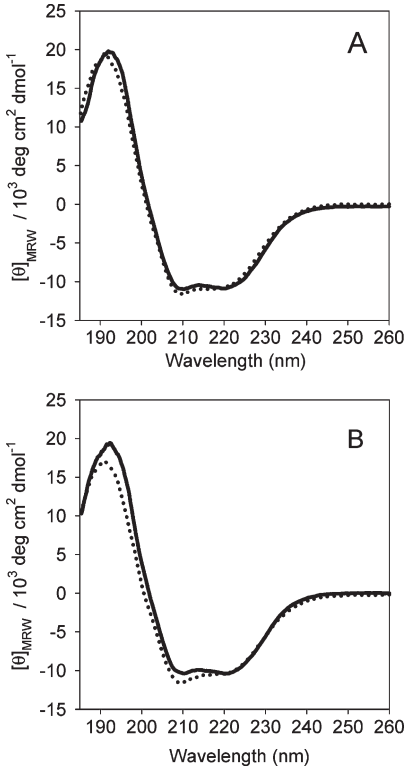

FIGURE 2: The structure of PrP mutants. Far-UV CD spectra of (A) PrP^{Wt} (solid line) and PrP^{F197W} (dotted line) and (B) PrP^{Q167R} (solid line) and $PrP^{Q167R/F197W}$ (dotted line) at concentrations between 13.5 and 14 μM, pH 5.5.

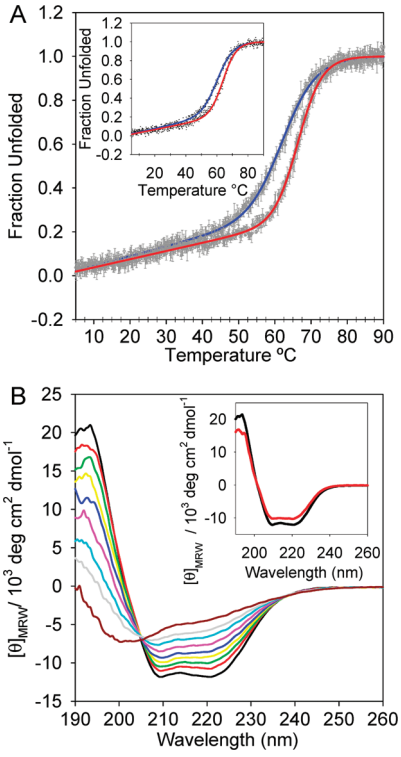

FIGURE 3: Thermal unfolding of PrP^{Wt} and PrP^{Q167R}. (A) Thermal unfolding transition curves of PrP^{Wt} (red) and PrP^{Q167R} (blue) measured by the changes in circular dichroism at 222 nm and normalized to fraction unfolded. Error bars show the standard deviation of three independent experiments. The inset shows the equivalent refolding transition curves. (B) Far-UV CD spectra of PrP^{Wt} at 5 (black), 40 (red), 55 (green), 60 (yellow), 62.5 (blue), 65 (magenta), 67.5 (cyan), 70 (gray), and 90 °C (brown). The inset shows the CD spectrum of PrP on recooling (red) overlaid with the initial spectrum at 5 °C (black).

Table 1: Thermodynamic Parameters for the Thermal Unfolding of PrP^{Wt} and PrP^{Q167R} [a]

PrP construct	ΔH/kJ mol^{-1}	T_m/°C
Wt	−291.4 ± 3.0	66.7 ± 0.3
Q167R	−200.0 ± 2.7	62.70 ± 0.03

[a]The enthalpy of unfolding (ΔH) and the temperature at which half the protein is unfolded (T_m) were calculated from the two-state analysis of the thermal unfolding transition curves. Thermodynamic parameters were calculated from the average of three separate experiments derived from CD measurements at 222 nm, and the errors represent the standard error.

thermal unfolding transition curves (Figure 3A) as this band is representative of α-helical structure. For both PrP^{Wt} and PrP^{Q167R} the major unfolding transition takes place over a narrow range of temperatures, which indicates that folding is a cooperative process. The transition curve for the Q167R mutant shifts to lower temperatures in comparison with the wild-type, as reflected by the lower value of the T_M and a decrease in ΔH (Table 1). These changes reflect a significant destabilization of the secondary structure of PrP^{Q167R} relative to PrP^{Wt}, with respect to thermal unfolding.

The spectral changes across the entire far-UV CD region were recorded at selected temperatures along the transition curves. A typical series of spectra for an unfolding experiment are shown in Figure 3B for PrP^{Wt}. The dominant features of the spectrum at 5 °C are negative bands at 208 and 222 nm and a positive band at 195 nm, which are characteristic of α-helix structure. On increasing temperature these three bands decrease in intensity, and a single negative band appears with a minimum around 200 nm, which is characteristic of random coil structure. The shape of the CD spectrum at 90 °C indicates that there is still some residual structure present, which was also observed for the chemical denaturation of the human prion protein (*21*). An isodichroic point is observed at ~205 nm, which provides strong evidence that the unfolding takes place as a two-state process without the accumulation of a stable intermediate. Similar spectral changes were observed for the Q167R mutant with the same gradual changes in the spectra on increasing temperature and the presence of the isodichroic point at 205 nm (data not shown).

To test the refolding of wild-type PrP and the Q167R mutant, the unfolding transition curves were reversed back to 5 °C (inset, Figure 3A). In addition, the far-UV CD spectrum was also recorded at 5 °C after unfolding at 90 °C. The spectrum re-forms its original shape on recooling, which indicates that protein folding is reversible (inset, Figure 3B). There is a slight drop in signal, which is probably due to the aggregation of protein at high temperatures, which is common for the thermal unfolding of proteins (*22*). Once normalized to take into account the aggregation of protein, the refolding transition curves are very similar to the unfolding curves, with a single cooperative refolding transition around the same temperatures as the unfolding transitions (inset, Figure 3A). Again, the destabilization conferred by the mutation is evident in the refolding experiments by the shift of the transition curve to lower temperatures.

Denaturant Unfolding of PrP^{F197W} and $PrP^{F197W/Q167R}$. Tryptophan fluorescence is highly sensitive to the local environment of the tryptophan residues; therefore, they are useful probes for monitoring changes in tertiary structure. The folding-sensitive tryptophan residue, W197, becomes solvent exposed when the protein unfolds, and this results in a red shift in the λ_{max} and a decrease in the fluorescence intensity (inset, Figure 4A). Both of these parameters can be followed to monitor folding. The denaturant unfolding transition curves of PrP^{F197W} and $PrP^{F197W/Q167R}$ derived from the red shift in λ_{max} are shown in Figure 4A. It can be seen for F197W that the major unfolding transition occurs between 5 and 8 M urea, and these data fit a cooperative two-state transition.

The unfolding curve of $PrP^{F197W/Q167R}$ also follows a cooperative two-state transition; however, the mutation results in a significant shift in the position of the transition region relative to the wild-type protein, as reflected by the difference in the midpoints of the transition (Table 2). As the Q167R mutant unfolds at lower urea concentrations, the mutation results in a significant destabilization of the protein as highlighted by the decrease in the free energy of unfolding. Transition curves plotted from the fluorescence intensities result in similar folding curves to those obtained by measuring the red shift (data not shown).

Denaturant unfolding of PrP was also monitored by changes in secondary structure measured by far-UV CD (Figure 4B). Unfolding transition curves were calculated from the change in the CD signal at 222 nm. Representative CD spectra for increasing concentrations of urea are shown in the inset of Figure 4B. The destabilization of the protein due to the presence of the Q167R mutation is also evident by the slight shift in the transition curve to lower urea concentrations (Figure 4B).

Unfolding of Mouse PrP Proceeds without the Accumulation of an Intermediate. The tryptophan fluorescence unfolding transitions overlay with the change in CD at 222 nm

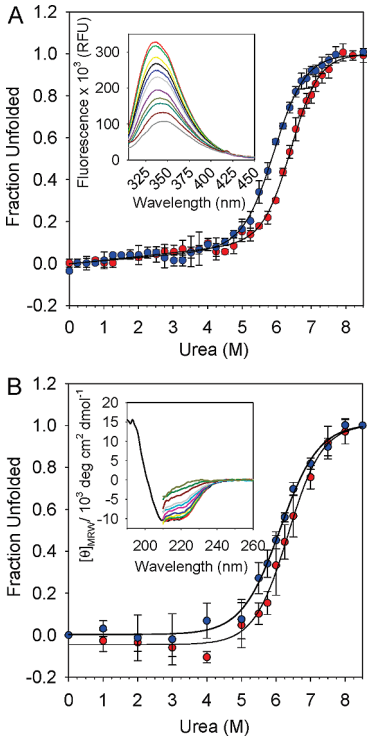

FIGURE 4: Denaturant unfolding transition curves of PrP^{F197W} and $PrP^{F197W/Q167R}$. Unfolding transition curves of PrP^{F197W} (red) and $PrP^{F197W/Q167R}$ (blue) at pH 7 monitored by (A) the red shift in tryptophan fluorescence and (B) the molar ellipticity at 222 nm, both of which were normalized to the fraction of unfolded protein. Error bars represent the standard deviation. The inset in panel A shows a representative series of tryptophan fluorescence spectra of PrP^{F197W} with urea concentrations of 0 (red), 4.25 (green), 4.75 (yellow), 5.24 (black), 5.5 (blue), 5.74 (gray), 5.97 (purple), 6.37 (gold), 6.55 (cyan), 6.86 (brown), and 7.3 M (gray). The inset in panel B shows a representative series of CD spectra of PrP^{F197W} with urea concentrations of 0 (black), 3.5 (red), 4.5 (green), 5.5 (yellow), 5.75 (blue), 6 (magenta), 6.25 (light blue), 6.5 (gray), 7 (brown), 7.5 (dark green), and 8.5 M (dark yellow).

Table 2: Thermodynamic Parameters for the Denaturant Unfolding of PrP^{Wt} and PrP^{Q167R} [a]

PrP construct	ΔG_0/kJ mol^{-1}	m/kJ mol^{-1} M^{-1}	$[D]_{50\%}$/M
F197W	-38.5 ± 2.6	6.0 ± 0.4	6.40 ± 0.02
F197W/Q167R	-32.2 ± 3.0	5.4 ± 0.5	5.9 ± 0.1

[a] The free energy of unfolding in the absence of urea (ΔG_0) and m values were calculated from the two-state analysis of fluorescence denaturant unfolding curves. $[D]_{50\%}$ is the concentration at which half of the protein is unfolded.

(Figure 5A,B), which indicates that the secondary structure folds concurrently with the tertiary structure. This provides evidence that the unfolding of mouse PrP occurs without the accumulation of a stable intermediate. The refolding of PrP was also tested in terms of the blue shift in the tryptophan fluorescence spectrum. The refolding curves overlap with the unfolding curves (Figure 5A,B), which show that refolding is reversible. Therefore, thermodynamic parameters were calculated from the unfolding curves derived from the red shift in tryptophan fluorescence (Table 2).

Phase diagram analysis for the unfolding of PrP^{F197W} and $PrP^{F197WQ167R}$ produced linear plots (Figure 5C). This shows that the unfolding is an all or none transition between the

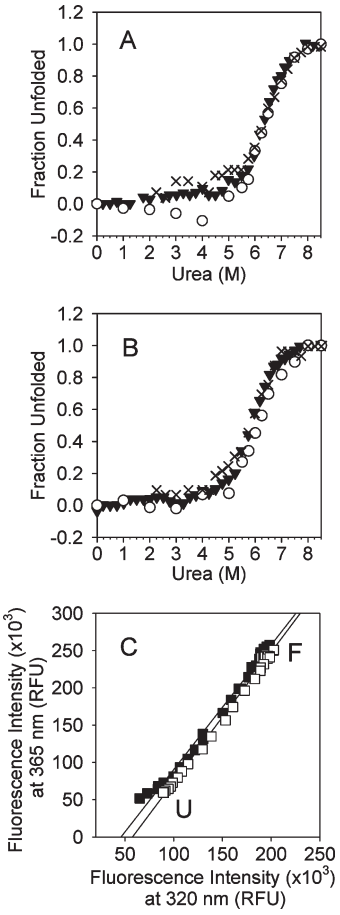

FIGURE 5: Unfolding of $MoPrP^{F197W}$ and $MoPrP^{F197W/Q167R}$ proceeds without the formation of a stable intermediate. PrP denaturant unfolding transition curves for (A) PrP^{F197W} and (B) $PrP^{F197W/Q167R}$ measured by fluorescence (triangles) and circular dichroism (circles). Crosses represent refolding experiments measured through fluorescence. Panel C shows phase diagram analysis of the unfolding of PrP^{F197W} (black squares) and $PrP^{F197W/Q167R}$ (white squares) plotted from the fluorescence intensities at 320 and 365 nm. The straight lines were fitted through linear regression.

folded and unfolded states without the formation of a stable intermediate.

DISCUSSION

For PrP^C to convert to its misfolded isoform, it must first partially unfold; therefore, gaining information on the unfolding properties of PrP may give insight into the mechanism of misfolding. The unfolding of mouse PrP fits a cooperative two-state transition, which is consistent with previous folding studies of mouse PrP using circular dichroism (*23*) and tryptophan fluorescence (*24*, *25*). Such studies used a different folding-sensitive mutant with the tryptophan residue located at position 175. The transition curves that are produced from both folding-sensitive mutants are almost identical, which indicates that folding is independent of the position of the single tryptophan residue used to monitor the process.

Disease-Resistant Q167R Mutant Destabilizes the Structure of PrP. The most noticeable effect of the Q167R mutation is the destabilization of the protein as shown by the shift of the unfolding transition in the thermal (Figure 3) and denaturant (Figure 4) experiments. Studies on the ovine prion protein with the equivalent mutation, Q171R (*26*−*28*), have also shown that the mutation destabilizes the secondary structure of

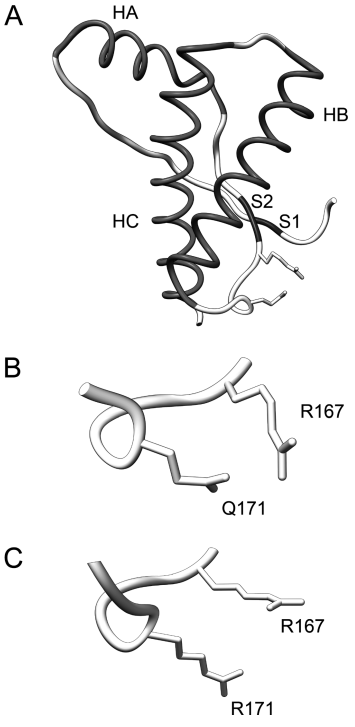

FIGURE 6: Crystal structures of ovine PrP codon 171 variants. Ribbon representations of (A) ovine PrP Q171 with the amino acids at positions 167 and 171 highlighted (sheep numbering) and the loop region (residues 167−173) of (B) the Q171 variant and (C) the R171 variant. The structures were drawn from the PDB files 1TPX (Q variant) and 1TQC (R variant) using Chimera as described in the legend for Figure 1.

PrP. Here we have shown that the disease-resistant Q167R mutation destabilizes mouse PrP in terms of both the secondary and tertiary structure (Figure 4), and this is the only detectable change we observe. This destabilization is surprising, considering that the mutation prevents disease, and structural destabilization makes unfolding and therefore misfolding more energetically favorable. This suggests that the stability of PrP does not always reflect its propensity to misfold *in vivo*, which is supported by the fact that not all disease-inducing mutations destabilize PrP (*29*). There must therefore be an alternative reason for the resistance induced by the Q167R mutation, which may be related to the destabilization that it confers. One possible explanation is that the mutant has a higher turnover in the cell, which lowers the pool of available PrP^{C} for conversion to PrP^{Sc}, and therefore makes the host less susceptible to disease.

A structural rationalization for the destabilization conferred by the disease-preventing mutation is evident from co-crystallization studies on both the resistant (ARR) and susceptible (ARQ) variants of ovine PrP (*30*) (Figure 6). In the ARQ variant a hydrogen bond exists between R167 and Q171 (sheep numbering), which stabilizes the loop region between strand S2 and helix HB. In the ARR variant R167 and R171 repel each other, which results in destabilization of the loop region. This interpretation is further supported by molecular dynamics simulations of the ovine variants (*31*), which indicate that the backbone in the loop region of residue 171 is destabilized in the ARR variant, which shortens strands S1 and S2 and therefore accounts for the experimental destabilization of the protein. The same explanation is relevant to the destabilization of mouse PrP as the same repulsion is likely to occur between residues R163 and R167 (mouse numbering), thus leading to destabilization of the loop region and shortening of the β-sheet. Furthermore, molecular dynamics simulations and hydrogen/deuterium exchange experiments on PrP have revealed large-scale fluctuations that involve the opening of the core of the protein between the S1-HA-S2 subdomain and the HB-HC subdomain, which are hinged by the S2-HB loop (*32*−*34*). The presence of the Q167R mutation is therefore likely to cause destabilization of the loop and promote the opening of the domains, resulting in destabilization of the global tertiary structure of the protein. This interpretation is supported by molecular dynamics simulations showing that disruption of a specific salt bridge in the loop of human PrP promotes the physical separation of these domains (*35*).

The flexibility of the loop region that links the S2 strand with helix B is emerging as an important factor in pathogenesis of prion disease. The NMR structure of the elk prion protein shows a highly defined loop region (*36*) which is disordered in other mammalian PrP structures, such as mouse and human (*37*, *38*). Changing two amino acids in the loop region of mouse PrP to those that are present in elk results in a rigid loop that resembles that of elk (*36*). Transgenic mice that mildly overexpress mouse PrP with this rigid loop contract a spontaneous prion disease (*39*, *40*), which on subsequent inoculation is infectious to mice that overexpress wild-type PrP. This indicates that amino acid substitutions that stabilize the loop region result in spontaneous prion disease in mice and yet amino acid substitutions that prevent disease in mice clearly destabilize this region. It therefore appears that the amino acids in this region and their influence on the stability of the loop region are an important factor in prion disease susceptibility.

Differences in Folding Properties of Mouse and Hamster PrP May Explain the Species Barrier. As we have previously studied the unfolding of the hamster prion protein, using the equivalent single tryptophan mutant (F197W) (*16*), direct comparisons between unfolding of mouse and hamster PrP can be made. The first noticeable feature is that the unfolding transition curves, monitored by the red shift in tryptophan fluorescence, show that the tertiary structure of hamster PrP unfolds at much lower urea concentrations compared to mouse PrP. This is reflected in the midpoint of the transitions being 3.4 M urea for the hamster and 6.4 M urea for the mouse. Other features include the noncoincidence of unfolding transition curves measured through fluorescence and circular dichroism and the presence of an intermediate that is detectable by two distinct linear transitions with a single intersection in the phase diagram analysis (*16*). This is in contrast to mouse PrP, where the transition curves overlay and the phase diagram analysis reveals a single linear all-or-none transition without an intermediate (Figure 5).

These data therefore reveal that the two proteins, which have very similar sequence and 3D structure, fold via very different mechanisms. The folding of hamster PrP follows a framework mechanism, where secondary structure elements form first, followed by tertiary structure acquisition through diffusion−collision (*41*). In contrast, the mouse prion protein folds through a nucleation condensation mechanism, where the secondary structure forms concurrently with the tertiary structure without the presence of a detectable intermediate (*42*). There are only eight amino acid differences between the mouse and hamster prion, and their structures are similar, so it is surprising that their folding mechanisms are so different. The most likely explanation for this is that the amino acid differences between mouse and hamster PrP influence the association of the S1-HA-S2 and the

HB-HC subdomains and therefore result in different mechanisms of tertiary structure acquisition. Variations in folding behavior between human PrP and its paralogue doppel have also been implied through molecular dynamics simulations (*43*), which therefore give another example of the variability in the folding process of prions and prion-like proteins. The difference in folding mechanisms highlighted in the present study is consistent with the fact that the fibrillization of hamster PrP is difficult under conditions that produce mouse PrP fibrils (*44*). Such fibrillization is under partially denaturing conditions; therefore, the difference in fibrillization properties can possibly be attributed to the different folding pathways involving different folding intermediate species. This fits with theories on the multiple routes to fibril formation (*45*), where the free energy barrier that separates the native and monomeric assembly-competent species is the determining factor in fibrillization kinetics.

There is a strong species barrier effect, in both directions, on transfer of infection between mice and hamsters (*46*), which manifests as a very long incubation time between infection and disease, if disease occurs at all. Experiments have shown that transgenic mice expressing hamster PrP are susceptible to infection by hamster prions, which shows that the species barrier is controlled by the primary sequence of the host PrP (*14*). Our results here display a clear difference in the folding properties of mouse and hamster PrP. It is well established that both the folding pathway and species barrier are controlled by the primary sequence of PrP, and so it is possible that the difference in the folding mechanism can explain the molecular basis of the species barrier.

Based on the differences between the folding pathways of mouse and hamster PrP, it is likely that a partially unfolded precursor to amyloid formation would have a different structure and stability between the two species. This hypothesis is supported by high-pressure NMR studies on the human and hamster prion proteins that revealed intermediate states with structural differences between the two species (*47*). According to the protein only hypothesis PrP^{Sc} autocatalytically converts PrP^{C} into PrP^{Sc} and must therefore lower the energy barrier that separates the correctly folded and the misfolded isoforms. It is possible that the difference in structure and stability of the partially folded precursor dictates the specificity of prion conversion. This would mean that hamster PrP^{Sc} can only bind and convert the hamster intermediate and that mouse PrP^{Sc} can only bind and convert a mouse intermediate. Therefore, the interaction between PrP^{Sc} and the partially unfolded precursor rather than the more structurally conserved fully folded PrP may explain the species barrier that exists for the transfer of infection between mouse and hamster.

The folding studies presented here have shown that the disease-resistant mutant Q167R is destabilized relative to the wild-type protein. The findings highlight a possible molecular mechanism for the resistant phenotype. Differences in the unfolding properties of mouse and hamster prion proteins have also shed some light on the molecular basis of the species barrier. It appears that intermediate species on the folding pathway of PrP are more distinct between species than the fully folded forms and are therefore more likely to be the determinants of the species barrier.

ACKNOWLEDGMENT

We thank the Molecular Biology Service and Biological Mass Spectrometry Facility in the Department of Biological Sciences, University of Warwick, for DNA sequencing and mass spectrometry analysis. We also thank Prof. David Brown, University of Bath, for providing the mouse PrP plasmid.

REFERENCES

1. Prusiner, S. B. (1998) Prions. *Proc. Natl. Acad. Sci. U.S.A. 95*, 13363–13383.
2. Mead, S. (2006) Prion disease genetics. *Eur. J. Hum. Genet. 14*, 273–281.
3. Goldmann, W. (2008) PrP genetics in ruminant transmissible spongiform encephalopathies. *Vet. Res. 39*, 30.
4. Westaway, D., Zuliani, V., Cooper, C. M., Da Costa, M., Neuman, S., Jenny, A. L., Detwiler, L., and Prusiner, S. B. (1994) Homozygosity for prion protein alleles encoding glutamine-171 renders sheep susceptible to natural scrapie. *Genes Dev. 8*, 959–969.
5. Belt, P. B., Muileman, I. H., Schreuder, B. E., Bos-de Ruijter, J., Gielkens, A. L., and Smits, M. A. (1995) Identification of five allelic variants of the sheep PrP gene and their association with natural scrapie. *J. Gen. Virol. 76* (Part 3), 509–517.
6. Clouscard, C., Beaudry, P., Elsen, J. M., Milan, D., Dussaucy, M., Bounneau, C., Schelcher, F., Chatelain, J., Launay, J. M., and Laplanche, J. L. (1995) Different allelic effects of the codons 136 and 171 of the prion protein gene in sheep with natural scrapie. *J. Gen. Virol. 76* (Part 8), 2097–2101.
7. Hunter, N. (2007) Scrapie: uncertainties, biology and molecular approaches. *Biochim. Biophys. Acta 1772*, 619–628.
8. Goldmann, W., Hunter, N., Smith, G., Foster, J., and Hope, J. (1994) PrP genotype and agent effects in scrapie: change in allelic interaction with different isolates of agent in sheep, a natural host of scrapie. *J. Gen. Virol. 75* (Part 5), 989–995.
9. Kaneko, K., Zulianello, L., Scott, M., Cooper, C. M., Wallace, A. C., James, T. L., Cohen, F. E., and Prusiner, S. B. (1997) Evidence for protein X binding to a discontinuous epitope on the cellular prion protein during scrapie prion propagation. *Proc. Natl. Acad. Sci. U.S. A. 94*, 10069–10074.
10. Perrier, V., Kaneko, K., Safar, J., Vergara, J., Tremblay, P., DeArmond, S. J., Cohen, F. E., Prusiner, S. B., and Wallace, A. C. (2002) Dominant-negative inhibition of prion replication in transgenic mice. *Proc. Natl. Acad. Sci. U.S.A. 99*, 13079–13084.
11. Caplazi, P. A., O'Rourke, K. I., and Baszler, T. V. (2004) Resistance to scrapie in PrP ARR/ARQ heterozygous sheep is not caused by preferential allelic use. *J. Clin. Pathol. 57*, 647–650.
12. Lee, C. I., Yang, Q., Perrier, V., and Baskakov, I. V. (2007) The dominant-negative effect of the Q218K variant of the prion protein does not require protein X. *Protein Sci. 16*, 2166–2173.
13. Beringue, V., Vilotte, J. L., and Laude, H. (2008) Prion agent diversity and species barrier. *Vet. Res. 39*, 47.
14. Scott, M., Foster, D., Mirenda, C., Serban, D., Coufal, F., Walchli, M., Torchia, M., Groth, D., Carlson, G., and DeArmond, S. J.; et al. (1989) Transgenic mice expressing hamster prion protein produce species-specific scrapie infectivity and amyloid plaques. *Cell 59*, 847–857.
15. Chiti, F., and Dobson, C. M. (2009) Amyloid formation by globular proteins under native conditions. *Nat. Chem. Biol. 5*, 15–22.
16. Jenkins, D. C., Sylvester, I. D., and Pinheiro, T. J. (2008) The elusive intermediate on the folding pathway of the prion protein. *FEBS J. 275*, 1323–1335.
17. Gill, S. C., and von Hippel, P. H. (1989) Calculation of protein extinction coefficients from amino acid sequence data. *Anal. Biochem. 182*, 319–326.
18. Greenfield, N. J. (2006) Using circular dichroism collected as a function of temperature to determine the thermodynamics of protein unfolding and binding interactions. *Nat. Protoc. 1*, 2527–2535.
19. Santoro, M. M., and Bolen, D. W. (1988) Unfolding free energy changes determined by the linear extrapolation method. 1. Unfolding of phenylmethanesulfonyl alpha-chymotrypsin using different denaturants. *Biochemistry 27*, 8063–8068.
20. Kuznetsova, I. M., Turoverov, K. K., and Uversky, V. N. (2004) Use of the phase diagram method to analyze the protein unfolding-refolding reactions: fishing out the "invisible" intermediates. *J. Proteome Res. 3*, 485–494.
21. Hosszu, L. L., Wells, M. A., Jackson, G. S., Jones, S., Batchelor, M., Clarke, A. R., Craven, C. J., Waltho, J. P., and Collinge, J. (2005) Definable equilibrium states in the folding of human prion protein. *Biochemistry 44*, 16649–16657.
22. Evans, P., Slingsby, C., and Wallace, B. A. (2008) Association of partially folded lens betaB2-crystallins with the alpha-crystallin molecular chaperone. *Biochem. J. 409*, 691–699.

23. Liemann, S., and Glockshuber, R. (1999) Influence of amino acid substitutions related to inherited human prion diseases on the thermodynamic stability of the cellular prion protein. *Biochemistry 38*, 3258–3267.
24. Wildegger, G., Liemann, S., and Glockshuber, R. (1999) Extremely rapid folding of the C-terminal domain of the prion protein without kinetic intermediates. *Nat. Struct. Biol. 6*, 550–553.
25. Martins, S. M., Chapeaurouge, A., and Ferreira, S. T. (2003) Folding intermediates of the prion protein stabilized by hydrostatic pressure and low temperature. *J. Biol. Chem. 278*, 50449–50455.
26. Rezaei, H., Choiset, Y., Eghiaian, F., Treguer, E., Mentre, P., Debey, P., Grosclaude, J., and Haertle, T. (2002) Amyloidogenic unfolding intermediates differentiate sheep prion protein variants. *J. Mol. Biol. 322*, 799–814.
27. Rezaei, H., Marc, D., Choiset, Y., Takahashi, M., Hui Bon Hoa, G., Haertle, T., Grosclaude, J., and Debey, P. (2000) High yield purification and physico-chemical properties of full-length recombinant allelic variants of sheep prion protein linked to scrapie susceptibility. *Eur. J. Biochem. 267*, 2833–2839.
28. Paludi, D., Thellung, S., Chiovitti, K., Corsaro, A., Villa, V., Russo, C., Ianieri, A., Bertsch, U., Kretzschmar, H. A., Aceto, A., and Florio, T. (2007) Different structural stability and toxicity of PrP-(ARR) and PrP(ARQ) sheep prion protein variants. *J. Neurochem. 103*, 2291–2300.
29. Horiuchi, M., and Caughey, B. (1999) Prion protein interconversions and the transmissible spongiform encephalopathies. *Structure 7*, R231–R240.
30. Eghiaian, F., Grosclaude, J., Lesceu, S., Debey, P., Doublet, B., Treguer, E., Rezaei, H., and Knossow, M. (2004) Insight into the PrPC→PrPSc conversion from the structures of antibody-bound ovine prion scrapie-susceptibility variants. *Proc. Natl. Acad. Sci. U.S.A. 101*, 10254–10259.
31. Bujdoso, R., Burke, D. F., and Thackray, A. M. (2005) Structural differences between allelic variants of the ovine prion protein revealed by molecular dynamics simulations. *Proteins 61*, 840–849.
32. De Simone, A., Zagari, A., and Derreumaux, P. (2007) Structural and hydration properties of the partially unfolded states of the prion protein. *Biophys. J. 93*, 1284–1292.
33. Chebaro, Y., and Derreumaux, P. (2009) The conversion of helix H2 to beta-sheet is accelerated in the monomer and dimer of the prion protein upon T183A mutation. *J. Phys. Chem. B 113*, 6942–6948.
34. Eghiaian, F., Daubenfeld, T., Quenet, Y., van Audenhaege, M., Bouin, A. P., van der Rest, G., Grosclaude, J., and Rezaei, H. (2007) Diversity in prion protein oligomerization pathways results from domain expansion as revealed by hydrogen/deuterium exchange and disulfide linkage. *Proc. Natl. Acad. Sci. U.S.A. 104*, 7414–7419.
35. DeMarco, M. L., and Daggett, V. (2007) Molecular mechanism for low pH triggered misfolding of the human prion protein. *Biochemistry 46*, 3045–3054.
36. Gossert, A. D., Bonjour, S., Lysek, D. A., Fiorito, F., and Wuthrich, K. (2005) Prion protein NMR structures of elk and of mouse/elk hybrids. *Proc. Natl. Acad. Sci. U.S.A. 102*, 646–650.
37. Riek, R., Hornemann, S., Wider, G., Billeter, M., Glockshuber, R., and Wuthrich, K. (1996) NMR structure of the mouse prion protein domain PrP(121−321). *Nature 382*, 180–182.
38. Zahn, R., Liu, A., Luhrs, T., Riek, R., von Schroetter, C., Lopez Garcia, F., Billeter, M., Calzolai, L., Wider, G., and Wuthrich, K. (2000) NMR solution structure of the human prion protein. *Proc. Natl. Acad. Sci. U.S.A. 97*, 145–150.
39. Sigurdson, C. J., Nilsson, K. P., Hornemann, S., Heikenwalder, M., Manco, G., Schwarz, P., Ott, D., Rulicke, T., Liberski, P. P., Julius, C., Falsig, J., Stitz, L., Wuthrich, K., and Aguzzi, A. (2009) De novo generation of a transmissible spongiform encephalopathy by mouse transgenesis. *Proc. Natl. Acad. Sci. U.S.A. 106*, 304–309.
40. Soto, C. (2009) Constraining the loop, releasing prion infectivity. *Proc. Natl. Acad. Sci. U.S.A. 106*, 10–11.
41. Kim, P. S., and Baldwin, R. L. (1982) Specific intermediates in the folding reactions of small proteins and the mechanism of protein folding. *Annu. Rev. Biochem. 51*, 459–489.
42. Daggett, V., and Fersht, A. R. (2003) Is there a unifying mechanism for protein folding? *Trends Biochem. Sci. 28*, 18–25.
43. Settanni, G., Hoang, T. X., Micheletti, C., and Maritan, A. (2002) Folding pathways of prion and doppel. *Biophys. J. 83*, 3533–3541.
44. Breydo, L., Bocharova, O. V., Makarava, N., Salnikov, V. V., Anderson, M., and Baskakov, I. V. (2005) Methionine oxidation interferes with conversion of the prion protein into the fibrillar proteinase K-resistant conformation. *Biochemistry 44*, 15534–15543.
45. Thirumalai, D., Klimov, D. K., and Dima, R. I. (2003) Emerging ideas on the molecular basis of protein and peptide aggregation. *Curr. Opin. Struct. Biol. 13*, 146–159.
46. Kimberlin, R. H., Cole, S., and Walker, C. A. (1987) Temporary and permanent modifications to a single strain of mouse scrapie on transmission to rats and hamsters. *J. Gen. Virol. 68* (Part 7), 1875–1881.
47. Kremer, W., Kachel, N., Kuwata, K., Akasaka, K., and Kalbitzer, H. R. (2007) Species-specific differences in the intermediate states of human and Syrian hamster prion protein detected by high pressure NMR spectroscopy. *J. Biol. Chem. 282*, 22689–22698.
48. Pettersen, E. F., Goddard, T. D., Huang, C. C., Couch, G. S., Greenblatt, D. M., Meng, E. C., and Ferrin, T. E. (2004) UCSF Chimera—a visualization system for exploratory research and analysis. *J. Comput. Chem. 25*, 1605–1612.